JOURNAL OF PROPULSION AND POWER
Vol. 10, No. 2, March–April 1994

Incipient Torsional Stall Flutter Aerodynamic Experiments on Three-Dimensional Wings

Peter F. Lorber* and Franklin O. Carta†
United Technologies Research Center, East Hartford, Connecticut 06108

The aerodynamics of small amplitude pitching motions near stall have been studied experimentally in order to improve understanding of torsional stall flutter. A model wing was oscillated in pitch at several small amplitudes over a wide range of conditions. Unsteady surface pressures were measured and integrated to determine the aerodynamic damping at five spanwise stations. Attached flow damping was positive and, for moderate Mach numbers and frequencies, in good agreement with thin airfoil theory. Strong negative damping was found for motions centered near static stall for all studied reduced frequencies, Mach numbers, and sweep angles. The 30-deg swept-back configuration was found to become negatively damped over the entire span nearly simultaneously, while the unswept model exhibited local regions of negative damping that moved toward the wingtip as the mean angle of attack was increased.

Nomenclature

A = pitch rate, $\dot{\alpha}c/2U_c$
C_L = section lift coefficient, L/qc
C_M = section quarter-chord moment coefficient, M/qc^2
C_P = pressure coefficient, $(P - P_\infty)/q$
C_P^* = pressure coefficient for locally sonic chordwise velocity
c = airfoil chord, 17.3 in.
k = reduced frequency, $\omega c/2U_c$
L = aerodynamic lift
M = aerodynamic moment
M_c = chordwise Mach number, $M_\infty \cos \Lambda$
M_∞ = freestream Mach number
q = dynamic pressure, $\frac{1}{2}\rho_\infty U_c^2$
Re = Reynolds number, cU_c/ν
T = oscillation period
t = time
U_c = chordwise component of freestream velocity, $U_\infty \cos \Lambda$
U_∞ = freestream velocity
x = distance along chord from leading edge
z = distance along span from tip leading edge
α = geometric angle of attack, $\alpha_0 - \alpha_1 \cos \omega t$
α_{ss} = steady-state stall angle
Λ = sweep-back angle
ν = kinematic viscosity
Ξ = damping coefficent, Eq. (2)
ρ_∞ = freestream density
τ = nondimensional time, t/T
ω = circular frequency, $2\pi/T$

Introduction

AN experiment has been performed to investigate the aerodynamics of small amplitude pitching oscillations near static stall. The motivation for this research is the self-induced torsional stall flutter problem experienced by propeller blades. The instability may be encountered during high thrust static testing or at the start of the takeoff roll, when the blades are operating at high angles of attack. The characteristic behavior includes a small amplitude initiation, a rapid growth to a large amplitude, and a reduction in growth rate to establish a constant amplitude, limit-cycle oscillation. Early phenomenological studies[1–3] used strain gauges to record the decay or growth of the airfoil torsional response, but were unable to determine the actual aerodynamic damping or characterize the underlying physical mechanism. The related problem of dynamic stall of helicopter rotor blades was studied, starting in the 1960s, by measuring aerodynamic loads during forced large amplitude motions.[4–6] It is now possible to accurately measure unsteady blade pressures and obtain aerodynamic damping coefficients. A preliminary experiment[7] made such pressure measurements on a two-dimensional airfoil model oscillating in pitch at amplitudes of 0.5, 2.0, and 4.0 deg. The strongest negative (unstable) damping coefficients were found near the static stall angle for amplitudes of 0.5 and 2.0 deg. The measured damping coefficients were then applied in a simple model problem to compute the behavior of a single degree-of-freedom torsional oscillation. The predicted rapid growth to a limit cycle oscillation was similar to the early stall flutter results.

The initial experiment[7] used a nominally two-dimensional model, and was limited to relatively low Reynolds number, Mach number, and frequency ($Re = 6.5 \times 10^5$, $M_\infty = 0.18$, and $k \leq 0.16$). The small wind tunnel had less than ideal flow quality (relatively high turbulence level and unknown angularity), resulting in an earlier than anticipated static stall (9.5 deg). A more sophisticated experiment has now been conducted with a larger model and wind tunnel, with significantly improved instrumentation, and over a much wider range of conditions. This article describes the new experiment and presents a selection of the results. The effects of six independent parameters (Mach number, mean angle of attack, oscillation amplitude, reduced frequency, sweep angle, and spanwise position) are discussed, and a conceptual model is provided. It is hoped that this information will facilitate the design of lightweight propellers that avoid potential instabilities but do not require excessive stiffness.

Description of Experiment

The current model is a straight, untwisted, semispan wing of 17.3-in. (44-cm) chord and 48-in. (122-cm) span (Fig. 1), producing an aspect ratio of 5.6. The wing consists of a steel spar and fiberglass airfoil panels, and uses a Sikorsky SSC-

Received March 4, 1991; presented as Paper 91-0935 at the AIAA 32nd Structures, Structural Dynamics, and Materials Conference, Baltimore, MD, April 8–10, 1991; revision received April 2, 1993; accepted for publication July 2, 1993.

*Research Engineer. Senior Member AIAA.
†Supervisor, Experimental and Analytical Aeromechanics. Associate Fellow AIAA.

Table 1 Test matrix: number of amplitude and mean angle pairs

	Λ = 0			Λ = 15		Λ = 30		
k	M_c = 0.2	0.4	0.6	0.2	0.4	0.2	0.4	0.6
0.075					10			
0.10	9	15	10	11		9	21	18
0.20	25		6			34		13
0.25		9					8	
0.30	9					13		
0.40	9							
0.50						11		
0.60	4					13		

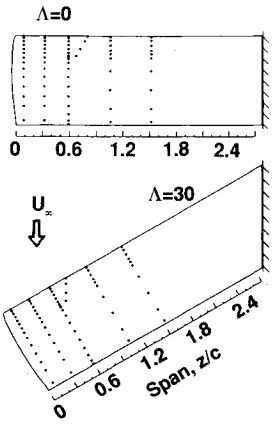

Fig. 1 Wing planform and transducer locations.

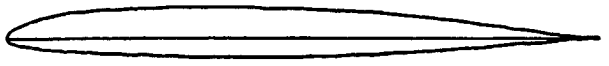

Fig. 2 SSC-A09 airfoil section.

A09 9% thickness cambered airfoil section (Fig. 2). The tip is rounded into an approximate body of revolution. The wing is mounted at sweep angles of 0, 15, and 30 deg from the side wall of the 8-ft (2.4-m) octagonal test section of the UTRC Large Subsonic Wind Tunnel. Additional airfoil panels are added to the spar at higher sweep angles in order to keep the wingtip quarter-chord at the tunnel centerline (Fig. 1). At Λ = 30 deg the span is increased to 55 in., an aspect ratio of 6.4. A hydraulic drive is used to oscillate the model in pitch about the line connecting the root and tip quarter-chord.

Unsteady surface pressure measurements were made on the wing model using 112 miniature transducers distributed among 5 spanwise stations. The suction surface transducer locations are shown by the dots in Fig. 1. The frequency response of the installed transducers has been measured by comparing their response to white noise with that of a reference microphone.[8] The initial resonance is typically between 4–12 kHz, well above the current range of interest (fundamental frequencies of up to 30 Hz). Steady-state calibration was performed over the full range of pressures (+2.5 to −12.5 psi) and temperatures (50–110°F) expected. This procedure[8,9] results in a steady-state calibration accuracy of better than 0.5% of the full-scale pressure range. Two bending and one torsional strain gauge bridges were mounted on the spar to verify that limit stresses were not exceeded and to allow wing deflections to be estimated. (The deflections were not significant for the conditions reported here.) The output of each sensor was digitized 1024 times during each of 40 pitching oscillations, recorded on digital magnetic tape, ensemble averaged, and converted to coefficient form. The pressures were integrated along the chord at each of the five spanwise stations to determine the unsteady lift, pressure drag, and pitching moment coefficients.

The incipient stall flutter work reported in this article is an element of a continuing program that is also studying large amplitude dynamic stall with application to helicopter rotors and maneuvering aircraft.[9,10] Table 1 shows the test matrix for the 260 incipient stall flutter data points. The test envelope included chordwise Mach numbers of 0.2, 0.4, and 0.6, corresponding to Reynolds numbers of 2, 4, and 6 × 10^6. Oscillation amplitudes of α_1 = 0.5, 1.0, and 2.0 deg were used. Additional steady state and α_1 = 6-deg results are also included in this article for comparison. The maximum oscillation frequency at these amplitudes was 30 Hz, corresponding to a reduced frequency of k = 0.6 at M_c = 0.2 and k = 0.2 at M_c = 0.6. These parameters are much more representative of the propeller operating environment than those used during the previous experiment.[7] The test conditions at each combination of M_c, Λ, and k were either (at the primary conditions) sets of up to 11 mean angles at a fixed amplitude, or (at secondary conditions) surveys of 3 mean angles (above, below, and equal to α_{ss}) at each amplitude.

Steady-State Results

Steady-state pressure distributions were measured at each Mach number and sweep angle, from zero angle of attack to beyond stall. In general, the results are in agreement with those expected for a simple subsonic wing. Of most relevance here are the effects of Mach number, sweep angle, and spanwise position on the stall characteristics. Figure 3 shows lift and pitching moment curves for the unswept wing at three Mach numbers for the furthest inboard station, z/c = 1.5. (Note that spanwise positions have been referenced to the wingtip to maintain constant values at the different sweep angles.) The stall angle, as determined from the break in the lift and moment curves, drops from 16.5 deg at M_c = 0.2, to 13 deg at M_c = 0.4, and to 10 deg at M_c = 0.6.

The standard infinite swept wing normalization was found to collapse C_L to a single curve for the inboard ($z/c > 0.3$) stations up to stall and at lower Mach numbers ($M_c < 0.4$). An example is shown in Fig. 4 for M_c = 0.2 and z/c = 1.06. Above stall, very close to the tip, or at higher Mach number, differences appear that are not accounted for by the simple normalization.[10,11]

The static stall angles, shown in Table 2, were determined from the lift and moment curves at each combination of M_c

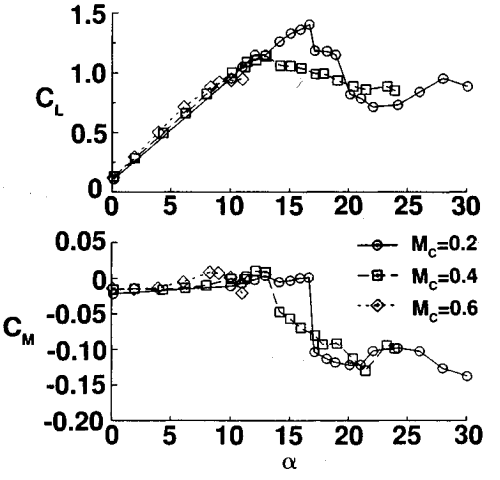

Fig. 3 Mach effects on steady lift and moment at Λ = 0 and z/c = 1.52.

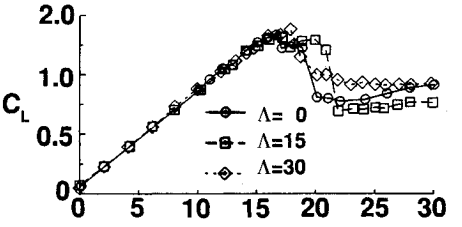

Fig. 4 Sweep effects on steady lift at M_c = 0.2.

Table 2 Steady-state stall angles

	Λ = 0			Λ = 15		Λ = 30		
z/c	M_c = 0.2	0.4	0.6	0.2	0.4	0.2	0.4	0.6
1.52	16.5	13	10	17	14.5	18	14	8
1.06	17	13.5	10	17	14.5	18	13	9
0.59	18	16	10.5	18	14.5	18	13	9
0.30	19	17	>11	18	15	18	13	9
0.08	>30	>30	>11	18	16	17.5	13	9

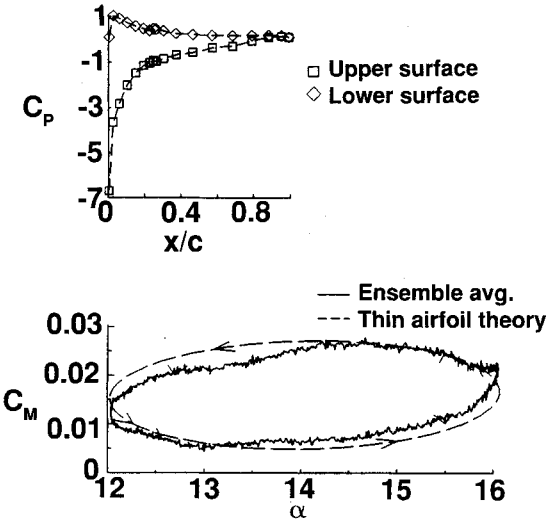

Fig. 5 Mean pressures and moment loop for attached flow at α = 14 − 2 cos ωt, M_c = 0.2, k = 0.2, Λ = 30 deg, and z/c = 0.59.

and Λ. The stall angle is significantly altered by the induced flow of the tip vortex: at Λ = 0 stall occurs from α = 2–4 deg higher at z/c = 0.3 than at z/c = 1.5. At z/c = 0.08 no stall was observed on the unswept wing over the range of tested angles of attack. At higher sweep angles the combination of spanwise flow and the inboard translation (Fig. 1) of the tip trailing edge relative to the leading edge causes the vortex to be quickly convected away from the tip. At Λ = 30 deg the variation of the stall angle with spanwise position is less than 1 deg.

Attached-Flow Oscillations

Small subsonic pitching oscillations that do not include penetration into stall are generally stable.[1-7] The unsteady component of the flow can usually be described using thin airfoil theory. For the simplest circumstances (two-dimensional, inviscid, and incompressible flow) Theodorsen's method[12,13] predicts an unsteady pitching moment about the quarter-chord of

$$C_M = -\alpha_1 k(\pi/2)(\sin \omega t + \tfrac{3}{8}k \cos \omega t) \qquad (1)$$

As described in Ref. 5, the out-of-phase first harmonic response (sin ωt) term makes the only contribution to the aerodynamic damping, which is therefore

$$\Xi = -\frac{1}{\pi\alpha_1^2}\oint C_M \, d\alpha = \frac{\pi k}{2} \qquad (2)$$

An example of an attached flow result of the current experiment is shown in Fig. 5. The conditions are α = 14 − 2 cos ωt, M_c = 0.2, Λ = 30, k = 0.2, and z/c = 0.59. The mean pressure distribution is smooth, with a strong suction peak of C_P = −6.8. Unsteady pressures (not shown) for this condition are characterized by smooth sinusoidal variations that are in phase with the angle of attack on the lower surface and 180 deg out of phase on the upper surface. The moment loop is elliptical, and exhibits counterclockwise motion (shown by the arrows), which corresponds to positive damping and stability.[5] The close match between the experimental unsteady moment and the thin airfoil result (the dashed ellipse) is typical of results at lower Mach numbers, lower reduced frequencies, and inboard stations. The slight tilt of the experimental ellipse axis is a quasisteady effect also present in the steady-state data (not shown). (Note that the experimental time-averaged C_M has been added to the thin airfoil result since the theory does not predict the steady moment.)

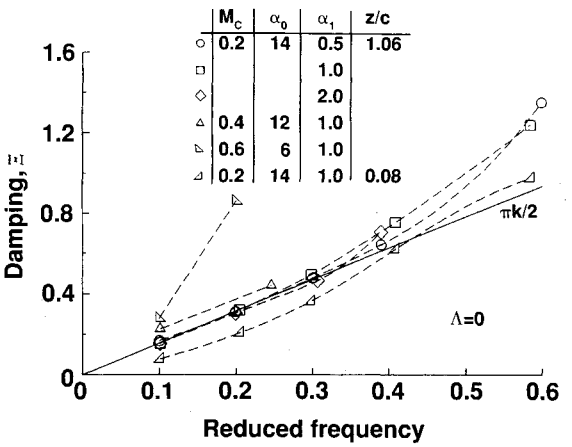

Fig. 6 Attached flow damping coefficients at Λ = 0.

Measured damping coefficients for several representative attached flow conditions are shown as symbols and dashed lines in Fig. 6. The theoretical prediction ($\pi k/2$) is a straight solid line. The experimental results at M_c = 0.2 and 0.4 follow the theory very well for $k \leq 0.4$ for all three amplitudes, but the experimental damping is substantially higher than the theory at k = 0.6, perhaps because its model of a straight, undistorted wake model is no longer adequate.[13] The experimental damping at M_c = 0.6 is also much higher than (πk/2), because the pressure distributions have become strongly affected by the presence of local supersonic flow. Very close to the wingtip, at z/c = 0.08, the experimental damping is smaller than the inboard result. These results have demonstrated a relatively wide range of conditions beyond incompressible, two-dimensional flow for which the simple theory continues to give acceptable results.

Oscillations near Static Stall

The situation changes abruptly when the flow contains substantial separation over a portion of the oscillation. As discussed in Ref. 7, the least stable conditions (the highest negative aerodynamic damping) are small amplitude oscillations centered about the static stall angle. This section will examine such a condition. Figure 7 shows the moment loop and pressure distributions for a 2-deg amplitude oscillation about the static stall angle of 18 deg, at M_c = 0.2, k = 0.3, Λ = 30, and z/c = 0.59. (Λ = 30 deg was chosen for clarity because the static stall angle is less dependent on spanwise position, reducing three-dimensional effects.) The experimental moment loop (the solid curve) shows a relatively constant moment ($C_M \simeq -0.05$) during the increase in angle from 16 to 20 deg, followed by a rapid drop to $C_M \simeq -0.14$ as the angle returns to 19 deg. The moment then recovers to $C_M \simeq -0.08$ by α = 16 deg. In comparison with the small ellipse predicted by thin airfoil theory (the dotted line), and with the attached flow loops (Fig. 5), this experimental loop is much larger and in the opposite (clockwise or unstable) sense.

The instantaneous pressure distributions in Fig. 7 illustrate the aerodynamic mechanism. Each is related to the corresponding point on the moment loop by the numbers 1–6. Near the start of the cycle, at τ = 0.1 (no. 1), the pressure distributions are similar to those in steady attached flow. In comparison with the fully attached flow (Fig. 5), the leading-edge suction load is reduced and the aft load increased, caus-

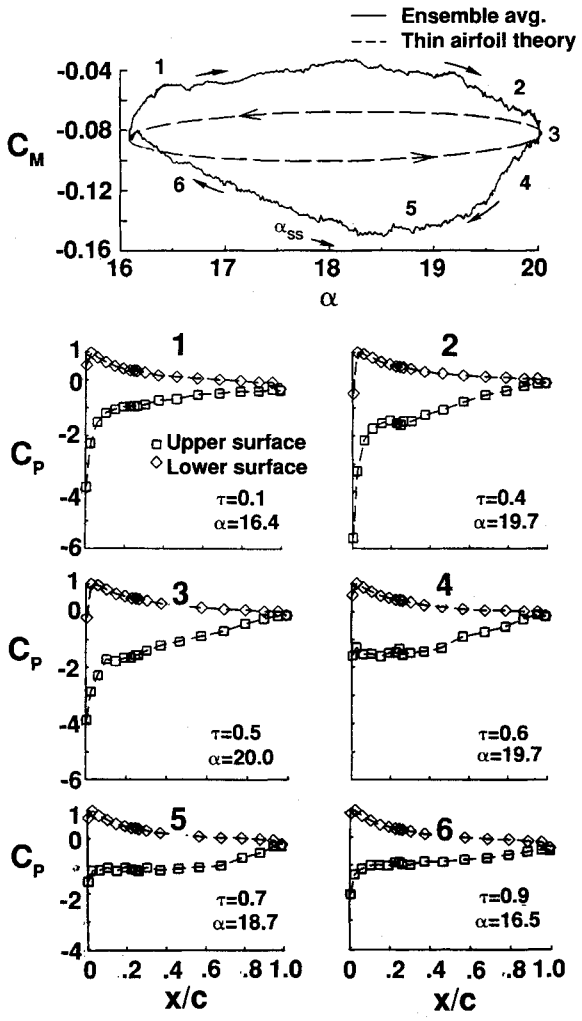

Fig. 7 Moment loop and instantaneous pressures for incipient separation for $\alpha = 18 - 2\cos\omega t$, $M_c = 0.2$, $k = 0.3$, $\Lambda = 30$ deg, and $z/c = 0.59$.

ing the moment to be negative rather than positive. The positive pitch rate allows a suction peak of up to $C_P \simeq -5.8$ to be maintained to $\alpha = 20$ deg (no. 2), 2 deg above static stall. This is the same basic mechanism that generates dynamic lift overshoots during large amplitude motions.[9] Since the instantaneous pitch rate for a sinusoidal oscillation is $A = \alpha_1 k \sin \omega t$, at maximum angle of attack the pitch rate is zero, and attached flow can no longer be maintained. The flow then separates near the leading edge (no. 3). The separation propagates back along the chord (no. 4) in the form of a small stall vortex, leading to massive separation by (no. 5). As the angle of attack drops further, reattachment occurs (no. 6), and the cycle repeats.

The large pressure distortions typical of dynamic stall[10] are not apparent here because the maximum pitch rate, $\alpha_1 k$, is 0.01, which generates only a weak stall vortex. The primary effect of separation is to create a negative (nose-down) moment during the second half of the cycle by removing the suction peak (which had contributed a nose-up moment), and increasing the loading at the trailing edge, (which adds a nose-down moment). The requirements for a strong instability are therefore 1) a minimum angle of attack low enough to maintain at least a locally attached flow at the leading edge during the initial portion of the cycle; 2) a pitch rate high enough to delay separation until the maximum angle is nearly reached; and 3) a maximum angle high enough so that when the positive pitch rate is removed, the flow separates and remains separated during much of the remainder of the cycle.

If the pitch rate is too low, the flow will separate and reattach near α_{ss}, and the required hysteresis will not be established. If the maximum and/or minimum angles are too high, the flow will either separate before the maximum angle is reached, or it will not reattach. In either case the necessary hysteresis will not be present. Since the pitch rate is determined by the product of frequency and oscillation amplitude, the minimum and maximum angles are determined by the sum of mean angle and amplitude, and the static stall angle is set by Mach number, sweep, airfoil geometry, and three-dimensionality, it is understandable that the experimental damping has a complex dependence on these parameters. These dependencies will now be described. Reference 11 contains an approximate empirical model for this behavior.

Mean Angle and Amplitude Effects

Both the mean angle and the amplitude have a major influence on the damping. Figure 8 illustrates this using curves of damping vs mean angle at $k = 0.2$, $M_c = 0.2$, $\Lambda = 30$, and $z/c = 0.59$ for three amplitudes: $\alpha_1 = 0.5$, 1, and 2 deg, and, at $k = 0.15$, for $\alpha_1 = 6$ deg. At very low amplitude ($\alpha_1 = 0.5$ deg) the region of negative damping is narrow and not very intense. Maximum negative damping values of $\Xi \simeq -0.2$ to -0.5 are typically found in a band approximately 0.5–1 deg wide that ends near $\alpha \simeq \alpha_{ss}$. At amplitudes of $\alpha_1 = 1$ and 2 deg, the negative damping band is wider (2–4 deg) and more intense ($\Xi \simeq -1.5$ to -2). At higher amplitudes ($\alpha_1 \geq 6$ deg) a less intense ($\Xi \simeq -0.5$) band of negative damping covers a 6- to 8-deg-wide region centered about α_{ss}. At all amplitudes considered here, the damping below the initial penetration into stall approaches a common value close to $(\pi k/2)$. The qualitative characteristics described here were also observed during the earlier experiment (cf. Fig. 9 in Ref. 7). Both sets of data indicate that the most unstable motions are 1–2-deg amplitude oscillations very close to α_{ss}.

Once the flow remains massively separated throughout the cycle, the damping is positive, and approaches a value slightly higher than in attached flow. This similarity between two very different flow regimes is interesting and worthy of further examination. The damping computed for the attached potential flow stems from three primary assumptions: 1) vorticity is shed from the trailing edge to maintain zero net circulation as the lift varies; 2) a Kutta condition is satisfied at the trailing edge (expressions of this condition include finite trailing-edge velocities, surface streamlines that are bounded by the airfoil trailing-edge angles, a smooth approach to zero pressure difference between the upper and lower surfaces, and an extended Kutta condition[14] that relates the difference in the upper and lower surface velocities to the time derivative of the circulation); and 3) an undistorted straight wake is convected downstream from the trailing edge at the freestream velocity.

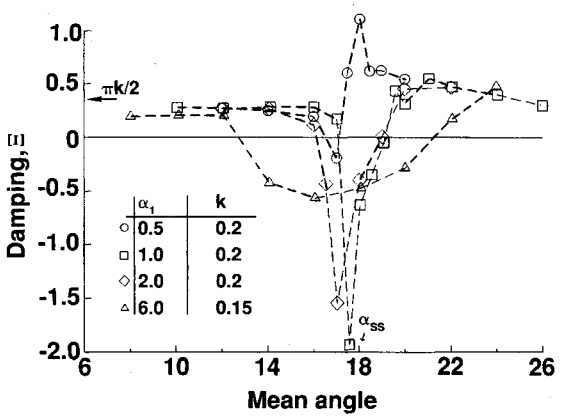

Fig. 8 Damping vs mean angle at several amplitudes for $M_c = 0.2$, $k = 0.2$, $\Lambda = 30$ deg, and $z/c = 0.59$.

The applicability of these three assumptions to small amplitude motions in separated flow will now be examined.

1) Lift variations of similar magnitude occur in both attached ($\alpha_0 = 16$ deg) and separated ($\alpha_0 = 22$ deg) conditions. Vorticity must therefore still be shed into the wake (although the shedding may not be restricted to the trailing edge).

2) The unsteady pressure results from the current experiment, as well as results[15] for a massively separated airfoil subject to flow angle oscillations at frequencies between $k = 0.5$ and 6.4, indicate that the unsteady pressures smoothly approach a common value at the trailing edge, satisfying at least one form of Kutta condition.

3) The assumption of an undistorted wake geometry is the least plausible. Even in attached flow, the wake distorts significantly from a straight line at high frequencies or large amplitudes. In massively separated flows vorticity is shed not in a thin wake emanating from the trailing edge, but throughout a broad region starting at the forward separation point.

It appears that even though there are violations in detail of the assumptions underlying the potential flow damping calculation, the fundamental similarity of shed vorticity and satisfaction of a trailing-edge condition is sufficient to generate damping values similar to attached flow.

Frequency Effects

In attached flow, increasing the reduced frequency was shown previously (Fig. 6) to produce a consistent and benign increase in damping. Such consistency is not present for unstable oscillations about the stall angle. This is illustrated in Fig. 9, which shows maximum negative damping coefficients plotted vs k. Each point represents the maximum measured negative damping over all values of α_0 for a particular combination of α_1, z/c, Λ, and M_c. Separate symbols are provided only for the different values of Λ. Figure 9 is not intended to provide comprehensive quantitative information, it is instead intended to illustrate trends:

1) For all reduced frequencies, damping coefficients of $\Xi < -1$ could be found for some combinations of α_0 and α_1.

2) The negative damping is generally weakest ($\Xi \simeq -1$) at $k = 0.1$, when the hysteresis is low.

3) The maximum negative damping is increased at $k = 0.2$–0.3 to $\Xi \simeq -1.5$ to -2.

4) For $k = 0.4$–0.5, and for most conditions at $k = 0.6$, the maximum negative damping is reduced to $\Xi \simeq -1.5$.

A somewhat different mechanism is involved in producing the very strong negative damping ($\Xi = -3$ and -5.8) measured at $k = 0.6$ and $\Lambda = 0$ (Fig. 9). At this frequency the maximum pitch rate is high enough ($A = 0.01$ for $\alpha_1 = 1$ deg) to generate a stall vortex. If the dynamics are similar to those at large amplitude,[9,10] the vortex forms near $(x_{sep}/c) = 0.15$ and convects downstream at $V \simeq 0.3U_\infty$. It will therefore remain above the wing for a time of

$$\Delta t = \frac{\Delta x}{V}, \qquad \Delta\tau = \frac{k}{2\pi}\frac{1 - (x_{sep}/c)}{(V/U_\infty)} \simeq 0.3 \tag{3}$$

A relatively high reduced frequency is therefore required for the vortex to remain above the wing for a significant fraction of the cycle. The effect of the stall vortex on the pressure distributions is shown in Fig. 10. Separation occurs after $\tau = 0.4$, and by $\tau = 0.8$ the vortex is above the trailing edge, generating large trailing-edge suction, a nose-down moment, and increased instability.

Mach Number Effects

In attached flow (Fig. 6) the damping at $M_c = 0.4$ is very similar both to the $M_c = 0.2$ data and to incompressible theory, while the damping at $M_c = 0.6$ is larger. As illustrated in Fig. 11, it is difficult to identify such a clear dependence on Mach number for the maximum negative damping in separated flow. As in Fig. 9, each point represents the maximum over a range of α_0 at a particular combination of α_1, z/c, Λ, and k. The data are for $k \simeq 0.1$ and $k \simeq 0.2$. The principal conclusion drawn from Fig. 11 is that maximum negative values of $\Xi = -1$ to -2 occur at all studied Mach numbers.

The mechanism for instability at higher Mach number is fundamentally the same as at lower Mach number. The details of the pressure distributions are, however, different. Figure 12 shows pressures at two instants during an $\alpha = 15 \pm 2$-deg oscillation at $k = 0.25$, $\Lambda = 30$ deg, and $M_c = 0.4$. There is a small region of mild supersonic flow ($C_P < C_P^*$) near the leading edge in attached flow at $\tau = 0.2$, and there is separation over the forward 40% of chord at $\tau = 0.4$. Reattachment occurs by $\tau = 0.8$ (not shown). Except for a reduction in the chordwise extent of the separation, these results are very similar to Fig. 7, for $M_c = 0.2$. At $M_c = 0.6$ there is a

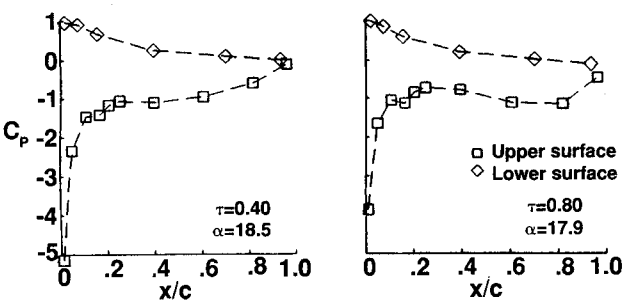

Fig. 10 Instantaneous pressure distributions showing the effect of a strong stall vortex at $M_c = 0.2$, $k = 0.6$, $\Lambda = 0$, $z/c = 1.52$, and $\alpha = 18 - 0.5 \cos \omega t$.

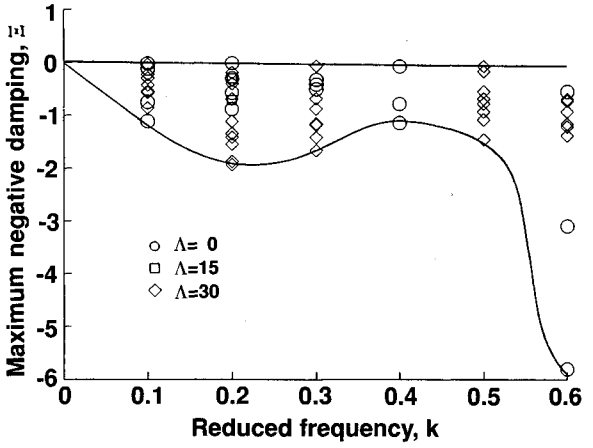

Fig. 9 Maximum negative damping coefficients as a function of reduced frequency.

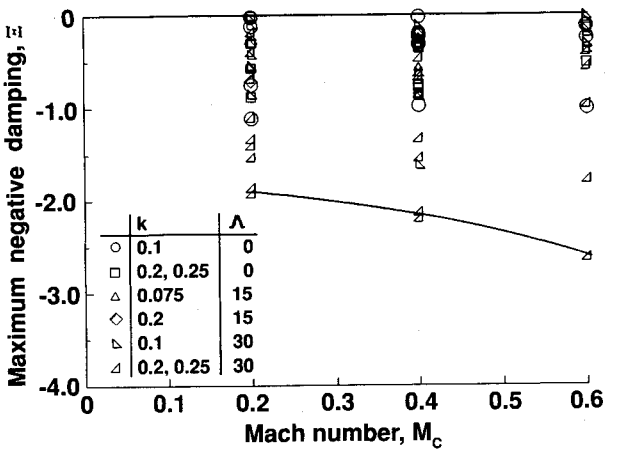

Fig. 11 Maximum negative damping coefficients as a function of Mach number.

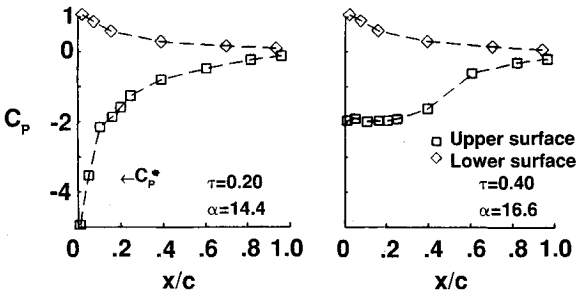

Fig. 12 Instantaneous pressure distributions showing incipient stall at $M_c = 0.4$, $k = 0.25$, $\Lambda = 30$ deg, $z/c = 1.06$, and $\alpha = 15 - 2 \cos \omega t$.

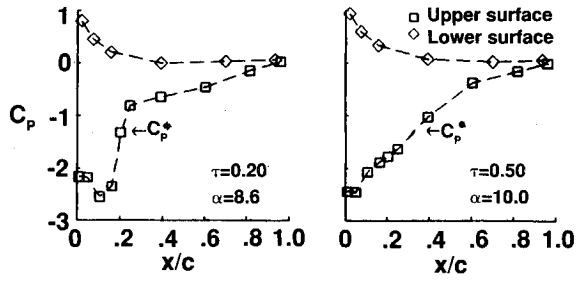

Fig. 13 Instantaneous pressure distributions showing incipient stall at $M_c = 0.6$, $k = 0.2$, $\Lambda = 30$ deg, $z/c = 1.06$, and $\alpha = 9 - 1 \cos \omega t$.

sizable supersonic region in high angle-of-attack attached flow, as shown in Fig. 13, for $\alpha = 9 \pm 1$ deg at $k = 0.2$. For $\tau < 0.2$, a maximum local chordwise Mach number of 1.5 is attained in a region that covers the front 20% of the chord. The region is terminated by a strong shock. A nose-up moment is created since the shock is ahead of $x/c = 0.25$. At $\tau = 0.5$ the flow has separated, and the shock is replaced by a region of highly random flow having (on average) a linear pressure gradient between $x/c = 0.05$ and 0.6. This change creates a nose-down moment. The flow reattaches near $\tau = 0.9$.

In terms of the moment loops, the detailed differences between the pressures at different values of M_c primarily alter the quasisteady and higher harmonic components. Since the damping depends only on the first harmonic, the damping changes little with M_c: $\Xi = -1.3$, -1.4, and -1.0 at $M_c = 0.2$, 0.4, and 0.6, respectively. It must be recognized that even though the strength of the instability is similar throughout the Mach number range studied, instability occurs at much lower angles of attack at higher Mach number, simply because the steady stall angle is lower (Table 2).

A second Mach effect is possible at higher reduced frequencies ($k \geq 0.6$). At large amplitude, compressibility has been observed to weaken the dynamic stall vortex.[9,10] If a similar weakening occurs at small amplitudes, the high negative damping observed at $k = 0.6$ and $M_c = 0.2$ may not be present for $M_c > 0.4$. This remains speculation, since no data for such conditions could be obtained in this experiment.

Sweep and Three-Dimensionality Effects

The fundamental requirement for negative damping is that the angle of attack passes through the steady stall angle during the cycle. It is not surprising that the differences in α_{ss} with spanwise position and sweep angle (Table 2) have a substantial influence on the local damping. Results for the unswept wing will be discussed first. Figure 14a shows contours of damping as a function of z/c and α_0 at $\Lambda = 0$, $M_c = 0.2$, $k = 0.2$, and $\alpha_1 = 1$ deg. The white circles and dashed lines show steady stall, $\alpha_{ss}(z)$, from Table 1. As α_0 is increased, negative damping first occurs inboard at $\alpha_0 = 16.6$ deg, and then moves outboard to $z/c = 0.30$ at $\alpha_0 = 22$ deg. The delay near the tip is caused by the lower effective angle of attack induced by the tip vortex. The entire wing is never simultaneously unstable, because the inboard region has returned to positive damping before the outboard region stalls. The station closest to the tip ($z/c = 0.08$) never stalls, and always has positive damping.

Results for equivalent conditions at $\Lambda = 15$ deg are shown in Fig. 14b. The instability again begins inboard, but for $\alpha_0 = 18$ and 19 deg the entire region outboard of $z/c = 1$ is unstable. The maximum instability lags approximately 1 deg behind α_{ss}. At $\Lambda = 30$ deg (Fig. 14c), the entire wing has

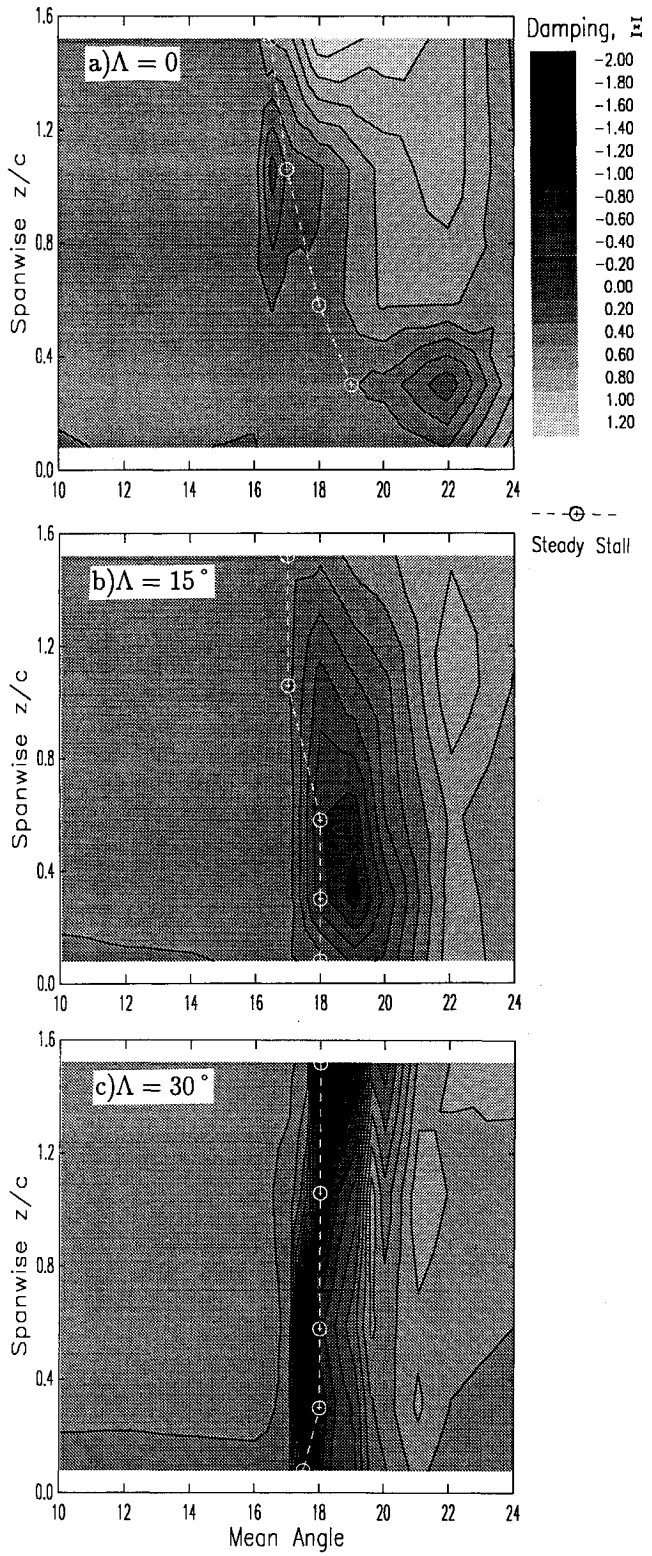

Fig. 14 Damping coefficients vs spanwise position for several mean angles, at $\alpha = \alpha_0 - 1 \cos \omega t$, $M_c = 0.2$, and $k = 0.2$.

negative damping for $17 \leq \alpha_0 \leq 19$ deg, a much more general instability than at lower sweep angles. The influence of the tip vortex is much weaker so that the local effective angles of attack are more uniform. All stations, including $z/c = 0.08$ have significant negative damping. Furthermore, the maximum negative damping is increased at all spanwise stations, probably because the simultaneous stall intensifies the local instabilities observed with no sweep.

Midchord Moments and Damping

The preceding discussion has been concerned with the damping coefficient computed using the pitching moment about $x/c = 0.25$. This was the model axis of rotation and the aerodynamic center of the SSC-A09 airfoil. However, the elastic axis for many propeller and turbomachinery blades is near $x/c = 0.50$. Therefore, damping information for midchord oscillations would be quite useful. Since the axis of rotation of our apparatus could not be moved, this section attempts to extrapolate from quarter-chord results using previous analytical and experimental results. In order to estimate the effects of changing the axis, the influence of two factors must be considered. The first is the change in the reference point about which the moment is computed. The second is the axis of the angular rotation.

The change in reference point adds $(\Delta x/c) = 0.25$ times the normal force coefficient to the instantaneous quarter-chord C_M. The quasisteady effect is to generate a moment that increases linearly with α prior to stall. In unsteady attached flow the effect is to reduce the positive damping, since normal force and lift loops generally have a clockwise sense, as shown in Fig. 9. The addition of a lift component is reflected in the analytical expression for the pitching moment[13] by the introduction of additional terms proportional to $C(k)$, the Theodorsen lift deficiency function.[12] The attached flow damping for oscillations about $x/c = 0.25$, using the moment referenced to $x/c = 0.5$ is

$$\Xi_{0.25,0.50} = (\pi/2)\{k[\tfrac{1}{2} - F(k)] - G(k)\} \qquad (4)$$

where F and G are the real and imaginary parts of $C(k)$. $\Xi_{0.25,0.50}$ will always be positive, but approaches zero at high frequency.

The effects of changing the moment reference point to midchord and recomputing the damping for the current experiment are illustrated in Fig. 15 for the same condition ($M_c = 0.2$, $k = 0.2$, $\Lambda = 30$) used in Fig. 8. The primary changes are a reduction in the attached flow damping [as predicted by thin airfoil theory, Eq. (4)], an earlier onset (by <1 deg) of negative damping, a small increase in the maximum negative damping, a broadening of the negative damping region above α_{ss}, and a reduction in the positive damping in poststall region. In general, changing the moment reference to midchord makes the aerodynamic damping more negative, but does not change the essential character of the phenomenon.

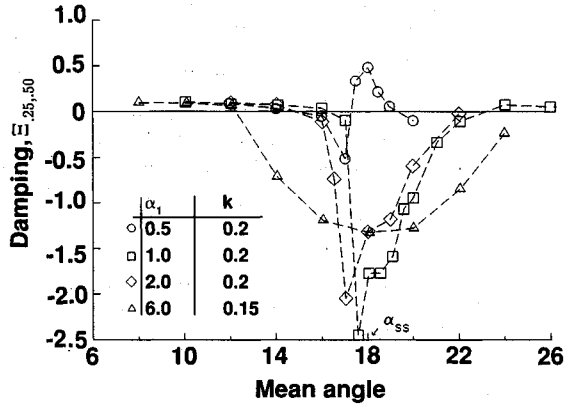

Fig. 15 Damping coefficient based upon midchord moment vs mean angle, at several amplitudes for $M_c = 0.2$, $k = 0.2$, $\Lambda = 30$ deg, and $z/c = 0.59$.

Previous studies of large amplitude separating flow have included different rotation axis locations. Ham and Garelick[16] reported that the maximum unsteady airload increments (and hence, the strength of the stall vortex), were not seriously changed by moving the pitch axis between $x/c = -0.25$ and $+0.75$. Stall was delayed the longest with the axis at the leading edge, and least with the axis at $x/c = 0.75$. In contrast, the more recent experiment of Helin and Walker[17] found that an aft axis location delayed dynamic stall and strengthened the vortex. The theoretical and analytical work of Jumper et al.[18] and the computational results of Visbal[19] indicate that at moderate pitch rates ($A < 0.025$) moving the pitch axis aft delays stall, but does not appreciably change the unsteady airloads.

The consensus appears to be that for moderate pitching rates, aft motion of the pitching axis will delay stall but leave the basic phenomenon relatively untouched. This implies that damping coefficients for motion about midchord should be similar to the quarter-chord results, but the mean angles of attack for maximum negative damping may be several degrees higher.

Conclusions

The primary results of this study of small amplitude pitching motions of a three-dimensional wing model are as follows:

1) The aerodynamic damping is positive for all studied motions where the instantaneous angle of attack remains below α_{ss}. For $k < 0.4$ and $M_c < 0.4$, the damping agrees with the results of incompressible thin airfoil theory, $\Xi = (\pi k/2)$. At higher frequencies or at $M_c = 0.6$, the damping is higher than $(\pi k/2)$. Very close to the wingtip, the damping is lower.

2) Small amplitude oscillations that include α_{ss} are usually unstable. The conditions for strong negative damping ($\Xi < -1$) include a positive pitch rate that delays stall beyond α_{ss}, a maximum angle high enough to cause separation, and a minimum angle low enough to permit at least local reattachment. Maximum negative damping was observed for 1- to 2-deg amplitude oscillations centered about α_{ss}, with $k > 0.2$.

3) For $k = 0.6$, the dynamic stall vortex is strong enough at low amplitude to significantly increase the trailing-edge loading. This generates a strong transient nose-down moment and increases the negative damping to $\Xi < -3$.

4) In fully separated flow the damping is positive, and somewhat larger in magnitude than in attached flow. This implies a degree of independence between the periodic, mean, and random flowfields.

5) Only differences in detail were observed between the $M_c = 0.2$, 0.4, and 0.6 results; the fundamental aerodynamic mechanism leading to negative damping is unchanged.

6) Sweep and spanwise position alter the aerodynamic damping primarily through changes in the local steady stall angle. For the unswept wing, stall and regions of negative damping occur at lower mean angles on the inboard portion of the wing (one chord or greater from the tip). As mean angle increases, stall moves outboard. Negative damping was never observed at the same instant over the entire wing. In contrast, at $\Lambda = 30$ deg, the wing stalled over its entire span within an angle-of-attack range of 1 deg. At $M_c = 0.2$, damping was negative over the entire span for a 2-deg-wide band centered at the static stall angle (18 deg).

In summation, this experiment has verified that torsional instability near stall occurs at realistic scales, and over a wide range of conditions. The underlying aerodynamic mechanism is sufficiently basic that negative aerodynamic pitch damping is possible whenever the local angle of attack is close to the local steady stall angle. Actual flutter will occur only if an initial excitation is present and if the structural natural frequency, stiffness, and damping permit. If the wing or blade is designed so that the stall angle varies sufficiently over its

span (as was true for the unswept model here), it may be possible to avoid global instabilities.

Acknowledgments

This research was funded by the NASA Lewis Research Center, as part of U.S. Army Research Office Contract DAAL03-89-C-0013. The authors would like to thank Alfred Covino for instrumenting the model and operating the data acquisition system during the test. We also thank John Ayer and the UTRC wind-tunnel staff for their assistance.

References

[1]Baker, J. E., "The Effects of Various Parameters, Including Mach Number, on Propeller-Blade Flutter, with Emphasis on Stall Flutter," NACA RML50L12b, 1950; reissued as NACA TN3557, 1955.

[2]Fanti, R., Carta, F. O., and Pitt, W. R., "Stall Flutter Characteristics of Several 16-Series Cantilevered Airfoil Models," United Aircraft Corp. Research Dept. Rept. R-23624-2, East Hartford, CT, May 1954.

[3]Lemmnios, A. Z., "Aerodynamic Damping Tests of Propeller Blade Airfoil Sections," United Aircraft Corporation Research Dept. Rept. R-0997-1, East Hartford, CT, Oct. 1957.

[4]Ham, N. D., "Stall Flutter of Helicopter Rotor Blades: A Special Case of the Dynamic Stall Phenomenon," *Journal of the American Helicopter Society*, Vol. 12, No. 4, 1967, pp. 40–48.

[5]Carta, F. O., and Niebanck, C. F., "Prediction of Rotor Instabilities at High Forward Flight Speeds. Volume III. Stall Flutter," USAAVLABS TR 68-18C, Ft. Eustis, VA, Feb. 1969.

[6]McCroskey, W. J., and Pucci, S. L., "Viscous Inviscid Interaction on Oscillating Airfoils in Subsonic Flow," AIAA Paper 81-0051, Jan. 1981.

[7]Carta, F. O., and Lorber, P. F., "Experimental Study of the Aerodynamics of Incipient Torsional Stall Flutter," *Journal of Propulsion and Power*, Vol. 3, No. 2, 1987, pp. 164–170.

[8]Marcolini, M. A., Lorber, P. F., Miller, W. T., and Covino, A. F., Jr., "Frequency Response Calibration of Recess-Mounted Pressure Transducers," Instrumentation Society of America 37th Annual Instrumentation Symposium, San Diego, CA, May 1991.

[9]Lorber, P. F., and Carta, F. O., "Airfoil Dynamic Stall at Constant Pitch Rate and High Reynolds Number," *Journal of Aircraft*, Vol. 25, No. 3, 1988, pp. 548–556.

[10]Lorber, P. F., Covino, A. F., Jr., and Carta, F. O., "Dynamic Stall Experiments on a Swept Three-Dimensional Wing in Compressible Flow," AIAA Paper 91-1795, June 1991.

[11]Lorber, P. F., Carta, F. O., and Covino, A. F., Jr., "An Oscillating Three-Dimensional Wing Experiment: Compressibility, Sweep, Rate, and Geometry Effects on Unsteady Separation and Dynamic Stall," United Technologies Research Center Rept. R92-958325-6, Contract DAAL03-89-C-0013, East Hartford, CT, Nov. 1992.

[12]Theodorsen, T., "General Theory of Aerodynamic Instability and the Prediction of Flutter," NACA Rept. 496, 1935.

[13]Bisplinghoff, R. L., Ashley, H., and Halfman, R. L., *Aeroelasticity*, Addison-Wesley, Reading, MA, 1955.

[14]Sears, W. R., "Unsteady Motion of Airfoils with Boundary Layer Separation," *AIAA Journal*, Vol. 14, No. 1, 1976, pp. 57–63.

[15]Covert, E. E., Lorber, P. F., and Vaczy, C. M., "Flow Separation Induced by Periodic Aerodynamic Interference," *Proceedings of the AFOSR/FJSRL/U. Colorado Workshop on Unsteady Separated Flows*, edited by M. S. Francis and M. W. Luttges, U.S.A.F. Academy, CO, Aug. 1983, pp. 169–176.

[16]Ham, N. D., and Garelick, M. S., "Dynamic Stall Considerations in Helicopter Rotors," *Journal of the American Helicopter Society*, Vol. 13, No. 2, 1968, pp. 49–55.

[17]Helin, H. E., and Walker, J. M., "Interrelated Effects of Pitch Rate and Pivot Point on Airfoil Dynamic Stall," AIAA Paper 85-0130, Jan. 1985.

[18]Jumper, E. J., Dimmick, R. L., and Allaire, A. J. S., "The Effect of Pitch Location on Dynamic Stall," *Forum on Unsteady Flow Separation, FED-Vol. 52*, American Society of Mechanical Engineers, New York, 1987, pp. 201–208.

[19]Visbal, M. R., "On Some Physical Aspects of Airfoil Dynamic Stall," American Society of Mechanical Engineers Symposium on Non-Steady Fluid Dynamics, Toronto, Canada, June 1990.